

Article

Effect of Operating Conditions on the Performance of Rh/TiO₂ Catalyst for the Reaction of LPG Steam Reforming

Aliko Kokka¹, Theodora Ramantani² and Paraskevi Panagiotopoulou^{1,*}

¹ School of Environmental Engineering, Technical University of Crete, GR-73100 Chania, Greece; akokka@isc.tuc.gr

² Department of Chemical Engineering, University of Patras, GR-26504 Patras, Greece; ramantani@chemeng.upatras.gr

* Correspondence: ppanagiotopoulou@isc.tuc.gr; Tel.: +30-28210-37770

Abstract: The catalytic performance of Rh/TiO₂ catalyst was investigated for the reaction of Liquefied Petroleum Gas (LPG) steam reforming with respect to the operating conditions employed. The impacts of reaction temperature, steam/C ratio, Gas Hourly Space Velocity (GHSV), and time were examined and discussed both in the absence and presence of butane in the feed. It was found that the catalytic performance is improved by increasing the reaction temperature, steam content in the feed, and/or by decreasing GHSV. In the presence of butane in the feed, the effect of H₂O/C ratio on catalytic performance is prominent, whereas the opposite was observed for the effect of GHSV. The propane conversion curve decreases by adding butane in the feed, indicating that the presence of butane retards propane steam reforming. The investigation of the dynamic response of Rh/TiO₂ catalyst to variations of H₂O/C ratio showed that neither catalytic activity nor product selectivity is varied with time following abrupt changes of the steam/C ratio between 2 and 7. The catalyst exhibited excellent stability with time-on-stream at 500 and 650 °C. However, a reversible catalyst deactivation seems to be operable when the reaction occurs at 600 °C, resulting in a progressive decrease of propane conversion, which, however, can be completely restored by increasing the temperature to 650 °C in He flow, respectively. The long-term stability of Rh/TiO₂ catalyst in the form of pellets showed that this catalyst is not only active and selective but also stable, and therefore, it is a promising catalyst for the reaction of LPG steam reforming.

Keywords: LPG steam reforming; H₂ production; Rh/TiO₂; GHSV; steam/C ratio; stability



Citation: Kokka, A.; Ramantani, T.; Panagiotopoulou, P. Effect of Operating Conditions on the Performance of Rh/TiO₂ Catalyst for the Reaction of LPG Steam Reforming. *Catalysts* **2021**, *11*, 374. <https://doi.org/10.3390/catal11030374>

Academic Editor: Valerie Dupont

Received: 18 February 2021

Accepted: 10 March 2021

Published: 12 March 2021

Publisher's Note: MDPI stays neutral with regard to jurisdictional claims in published maps and institutional affiliations.



Copyright: © 2021 by the authors. Licensee MDPI, Basel, Switzerland. This article is an open access article distributed under the terms and conditions of the Creative Commons Attribution (CC BY) license (<https://creativecommons.org/licenses/by/4.0/>).

1. Introduction

During the last decades, hydrogen (H₂) has attracted a lot of interest as a clean alternative energy source for the production of electricity via its electrochemical conversion in fuel cells, offering a viable alternative to fossil fuels [1–8]. Typical hydrogen production technologies include water electrolysis and steam reforming of several compounds such as natural gas, ethanol, methanol, glycerol, Liquefied Petroleum Gas (LPG), gasoline, and several oil-derived products [6,9–15]. Among various compounds, LPG is of special interest and is considered a suitable route for power generation via the intermediate production of H₂, especially in remote areas, where the existing power grids address serious problems (e.g., lack of natural gas infrastructure, high cost of modifying the existing infrastructure) [2,3,16,17]. LPG typically consists of propane (C₃H₈) and butane (C₄H₁₀) with various ratios depending on its source, recovery processes, and season, whereas small amounts of propylene and butylenes may also coexist [9,18–20]. For example, in the United States and Canada, LPG consists of at least 95% propane [18], whereas the composition of LPG in Australia varies between a 40:60 mixture of propane/butane to 100% of propane [19]. Although LPG is a gas mixture, it can be compressed to a transportable liquid at normal temperature in order to be safely transferred and stored [21].

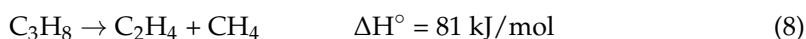
The high endothermicity of both propane and butane steam reforming reactions (Equations (1)–(4)) requires high temperatures (>700 °C) in order to achieve high H₂ yields.



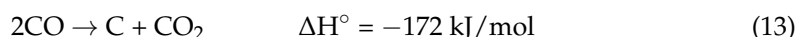
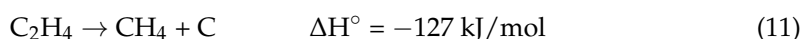
In addition to the above reactions (Equations (1)–(4)), the Water–Gas Shift (WGS) reaction (Equation (5)) often runs simultaneously in a manner that depends on reaction conditions and catalyst employed. The WGS reaction yields CO₂ and H₂ and is reversed at high temperatures due to thermodynamic restrictions.



In addition to H₂, CO, and CO₂, LPG can be converted to methane (CH₄), ethane (C₂H₆), and ethylene (C₂H₄), via the reaction of CO or CO₂ methanation (Equations (6) and (7)) and the decomposition of C₃H₈ (Equation (8)) and C₄H₁₀ (Equation (9)), respectively.



The major drawback of the LPG steam reforming process is carbon deposition due to the decomposition of C₂H₆, C₂H₄, CH₄, and CO (Equations (10)–(13)) [1,2,6,22]. This is enhanced by the possible presence of higher hydrocarbons in the initial LPG mixture, resulting in progressive catalyst deactivation.



Carbon formation can be suppressed either by controlling catalyst characteristics and reaction conditions, and/or by adding oxygen in the gas stream [6,16,23]. However, a number of issues should be addressed during the autothermal reforming process, including syngas oxidation and thus reduced hydrogen yields, operating restrictions, and safety problems [9,22]. Thus, recent investigations are focused on the development of active and stable catalysts that are able to convert LPG selectively to H₂, suppressing carbon deposition on the catalyst surface.

Previous studies have shown that Ni and Rh-based catalysts present high efficiency for the reaction of LPG steam reforming, and therefore, they have been widely studied [20,24–26]. The resistance toward carbon deposition can be improved by dispersion of the active phase on the surface of a reducible support such as CeO₂-ZrO₂, Gd doped-CeO₂, YSZ, or TiO₂ [2,9,21,22,27–29]. Based on mechanistic studies, the reactions proceed toward the dissociative adsorption of hydrocarbons on the surface of metal, followed by formation of CH_x species, which may be further dehydrogenated to hydrogen and carbon [2]. In case of catalysts supported on non-reducible metal oxides (e.g., Al₂O₃ or SiO₂), the so formed carbon may be accumulated on the metallic surface, resulting in catalyst deactivation. However, for catalysts supported on metal oxides characterized by high oxygen mobility

(e.g., CeO₂ or TiO₂), carbon may react with the lattice oxygen of the support, resulting in CO production and suppressing carbon deposition [2,22]. Based on this redox scheme, the oxygen vacancies created are replenished by H₂O originating from the feed stream.

An alternative approach for improving the resistance toward carbon accumulation is the optimization of the operating parameters of the reaction. High steam/C or W/F ratios have been proposed to suppress carbon formation and improve the lifetime of catalyst [1,9,23]. Excess steam was found to favor the WGS reaction, resulting in higher H₂ and CO₂ production, and also the reforming of the intermediate that produced CH₄, C₂H₄, and C₂H₆, which are selectively converted to CO and H₂ rather than to carbon via the decomposition reactions described above (Equations (10)–(12)).

In our previous study, it was found that supported Rh catalysts present high activity and selectivity for the propane steam-reforming reaction, with Rh/TiO₂ being among catalysts exhibiting optimum performance [29]. Thus, in the present study, the effect of operating parameters (temperature, Gas Hourly Space Velocity (GHSV), H₂O/C molar ratio, and time) on the catalytic performance of 0.5%Rh/TiO₂ catalyst is investigated in an attempt to optimize reaction conditions and increase the process efficiency. The dynamic response of catalyst to variations of operating parameters was also examined and discussed. Since propane is the main component of the LPG mixture, part of the present study is focused on the propane steam reforming reaction. The addition of butane in the gas stream in ratios similar to those of the real LPG mixture is also investigated. Moreover, the long-term stability of Rh/TiO₂ catalyst in the form of pellets is examined under realistic reaction conditions. The novelty of the present study lies in the development of an active, selective, and stable Rh/TiO₂ catalyst of high durability in variations of operating condition and suitable for use in H₂ production via LPG steam reforming for fuel cell applications. The results of the present study can be used to design and develop a highly efficient process for electricity production, which can replace conventional energy sources in order to address the serious problem of the depletion of fossil fuel reserves and the environmental concerns induced by their use, such as air pollution and major climate changes.

2. Results and Discussion

2.1. Catalyst Characterization

Characterization of the freshly prepared 0.5 wt % Rh/TiO₂ catalyst (reduced with H₂ at 300 °C for 2 h) showed that its specific surface area (SSA) was 43 m² g⁻¹ (Table 1). Rhodium dispersion and mean crystallite size (*d*_{Rh}) determined by H₂ chemisorption measurements were found to be 92.1% and 1.2 nm, respectively.

Table 1. Characteristics of fresh and spent 0.5%Rh/TiO₂ catalysts.

0.5%Rh/TiO ₂	SSA ¹ (m ² /g)	Composition ² (% Rutile)	Primary Crystallite Size of TiO ₂ ³ (nm)	
			Anatase	Rutile
Fresh	43	17.3	21.2	34.0
Fresh 600 °C (3 h)	30	41	23	35.0
Spent 600 °C (56 h)	6.6	100.0	-	49.6

¹ Specific surface area, determined with the B.E.T. (Brunauer–Emmett–Teller) method. ² Percent rutile content, estimated with the use of Equation (S1). ³ Primary crystallite size of TiO₂ estimated from X-ray diffraction (XRD) line broadening with the use of Equation (S2).

The diffractogram obtained from the fresh Rh/TiO₂ catalyst is shown in Figure 1 (trace a). It is observed that the titanium dioxide support consisted of 82.7% anatase and 17.3% rutile. The mean primary crystallite size of TiO₂ (*d*_{TiO₂}), determined by X-ray diffraction (XRD) peak broadening, was found to be 21.2 nm for anatase and 34.0 nm for rutile phase (Table 1).

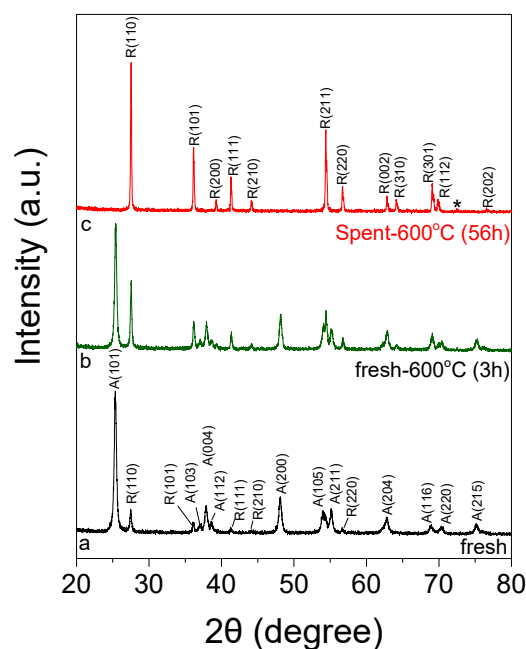


Figure 1. X-ray diffractograms of (a) fresh reduced, (b) fresh calcined in air at 600 °C followed by reduction at 300 °C and (c) spent 0.5%Rh/TiO₂ catalysts. Diffraction peaks denoted as “A”, “R”, and “*” are due to anatase TiO₂, rutile TiO₂, and graphite carbon phases, respectively.

No peaks assigned to Rh planes were detected in the XRD spectra due to the low Rh particle size estimated according to H₂ chemisorption.

2.2. Effect of Steam/C Ratio on Catalytic Performance

The effect of Steam/C ratio on catalytic performance was investigated for the propane steam reforming reaction over Rh/TiO₂ catalyst using a GHSV equal to 55,900 h⁻¹. The H₂O/C ratio was varied between 2 and 7 by varying the concentration of both C₃H₈ and H₂O in the gas stream in the range of 2.1–6.1% and 37–44%, respectively. Results obtained are presented in Figure 2, where propane conversion ($X_{C_3H_8}$) is plotted as a function of reaction temperature. It is observed that increasing the molar ratio of H₂O/C in the gas stream from 2 to 7 results in a progressive shift of propane conversion curve toward lower temperatures (by ≈70 °C).

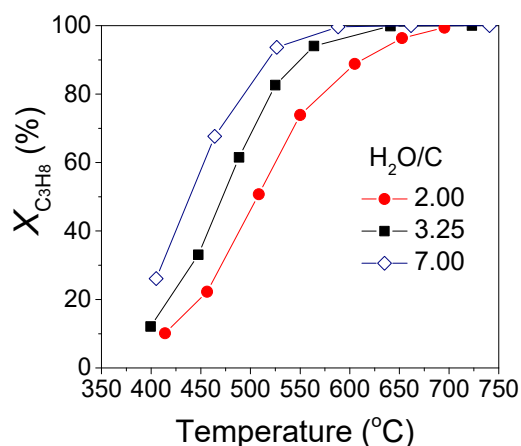


Figure 2. Effect of H₂O/C ratio on the conversion of C₃H₈ obtained as function of reaction temperature over 0.5%Rh/TiO₂ catalyst. Experimental conditions: Gas Hourly Space Velocity (GHSV): 55,900 h⁻¹; particle diameter: 0.15 < d_p < 0.25 mm; Feed composition: 2.1–6.1% C₃H₈, 0.15–0.20% Ar, 37–44% H₂O (balance He).

Product distribution obtained during interaction of the propane steam reforming mixture with the TiO₂-supported rhodium catalyst is strongly influenced by the molar ratio of steam/C in the feed. The results are presented in Figure 3, where it can be seen that in all cases, the main products detected are H₂, CH₄, CO, and CO₂. In the case of steam/C = 2 (Figure 3a), selectivity toward H₂ production (S_{H_2}) decreases from 96% to 79% with increasing temperature from 415 to 550 °C, and then it increases again to 95% with further increase of temperature at 700 °C. The decrease of S_{H_2} below 550 °C is accompanied by a decrease of CO₂ selectivity (S_{CO_2}) from 57% to 35% followed by CH₄ production, indicating that CO₂ methanation reaction takes place between 415 and 550 °C. Carbon monoxide hydrogenation may also result in CH₄ production as evidenced by the slight decrease of CO selectivity (S_{CO}) in the same temperature range. It should be noted that the hydrogenation of CH_x species that may be formed upon the dissociative adsorption of propane may also partially contribute to methane formation detected in Figure 3a.

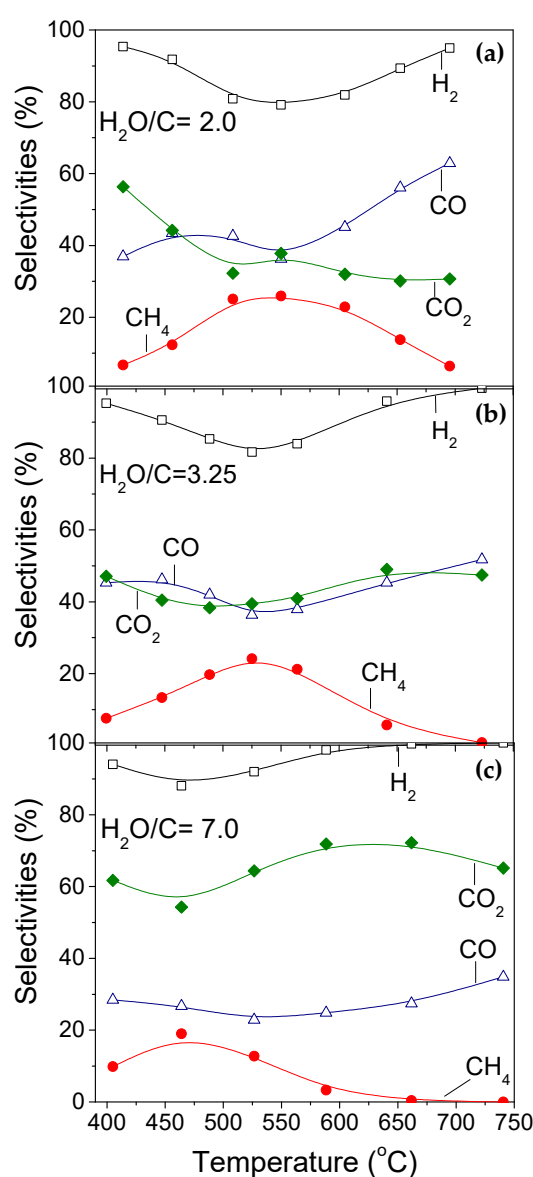


Figure 3. Effect of H₂O/C ratio on the selectivities toward reaction products obtained as a function of reaction temperature over 0.5%Rh/TiO₂ catalyst. (a) H₂O/C = 2; (b) H₂O/C = 3.25; (c) H₂O/C = 7. Experimental conditions: the same as in Figure 2.

At higher temperatures, S_{CO_2} decreases slightly, reaching 30% at 700 °C. It should be noted that selectivity toward CO_2 at 415 °C is higher (57%) than that of CO (36%), which is most possibly due to conversion of the produced CO toward CO_2 via the WGS reaction. However, S_{CO} progressively increases from 35 to 63% with increasing temperature from 550 to 700 °C, indicating that the WGS reaction is reversed above 550 °C in accordance to thermodynamic predictions [30]. Methane selectivity (S_{CH_4}) is generally lower than that of CO or CO_2 in the entire temperature range examined, going through a maximum value of 26% at 550 °C. The decrease of S_{CH_4} at higher temperatures, which is accompanied by an increase of both S_{CO} and S_{H_2} , is due to the occurrence of methane steam-reforming reaction, which is thermodynamically favored at high temperatures [31].

The increase of steam/C ratio in the feed results in the following differences in product distribution: (a) hydrogen selectivity at a given temperature increases with increasing steam concentration, whereas its decrease at low temperatures is lower as the steam/C ratio becomes higher, which is accompanied by lower methane selectivities. This implies that CO/CO_2 methanation reactions are suppressed with increasing H_2O concentration in the gas stream; (b) S_{CO} progressively decreases followed by an increase of S_{CO_2} , which is more pronounced at higher temperatures. This can be attributed to an enhancement of the WGS, CH_4 , and C_3H_8 steam-reforming reactions, which are well known to be thermodynamically favored over H_2O -rich gas streams [30,32,33].

The effect of steam/C ratio on the performance of Rh/TiO_2 catalyst was also investigated in the presence of butane in the gas stream using a ratio of propane/butane mixture equal to 95:5. The results obtained are presented in Figure 4, where the conversions of propane (Figure 4a) and butane (Figure 4b) are plotted as a function of reaction temperature.

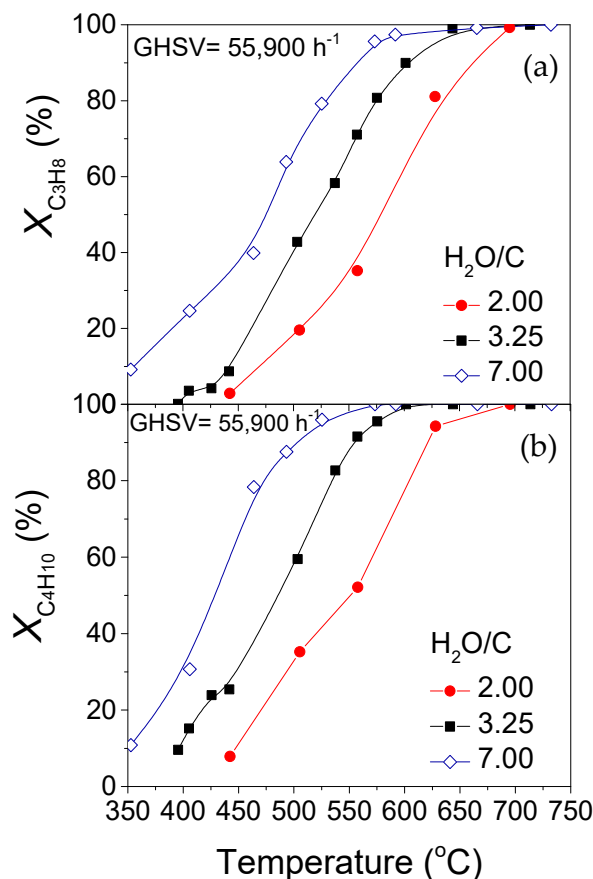


Figure 4. Effect of $\text{H}_2\text{O}/\text{C}$ ratio on the conversions of (a) C_3H_8 and (b) C_4H_{10} obtained as a function of reaction temperature over $0.5\% \text{Rh}/\text{TiO}_2$ catalyst. Experimental conditions: $\text{GHSV}: 55,900 \text{ h}^{-1}$; particle diameter: $0.15 < d_p < 0.25 \text{ mm}$; feed composition: 2.0–5.7% C_3H_8 , 0.1–0.3% C_4H_{10} , 0.15–0.20% Ar , 36.8–44.1% H_2O (balance He).

As it can be seen, the conversion curves of both C_3H_8 and C_4H_{10} are progressively shifted toward lower temperatures, by ≈ 110 and 130 °C, respectively, with increasing steam/C ratio from 2 to 7. A comparison of Figures 2 and 4 indicates that the improvement of catalytic activity with increasing steam content is higher in the presence of butane in the gas stream. However, it should be noted that propane conversion at a given temperature is significantly lower when the feed contains butane, indicating that its addition retards propane steam-reforming reaction. This may be attributed to the competitive adsorption of reactants on the same catalytically active sites in agreement with Al-Zuhair et al. [1], who reported that n-butane competes with propane, when they both coexist in the reaction mixture, and it blocks particular active sites.

The results of product distribution with temperature are shown in Figure S1, where it is observed that the products detected and trends observed with increasing H_2O content were similar with those discussed above in the absence of butane in the gas stream. A comparison of Figure 3 and Figure S1 exhibits the following differences: (a) S_{CO_2} at temperatures lower than 550 °C is generally higher in the presence of butane, whereas the opposite is observed for S_{CO} , indicating that the WGS reaction is favored using a C_3H_8/C_4H_{10} mixture in the feed. The enhancement of CO_2 production may be also due to the simultaneous occurrence of butane steam reforming (Equation (3)), which seems to be favored compared to Equation (4) due to the excess of H_2O in the feed; (b) the production of CH_4 is significantly lower when butane is present in the gas stream, indicating that either CO/CO_2 methanation reactions are suppressed or a parallel reaction is taking place resulting in methane consumption. This is supported by the higher S_{H_2} at temperatures lower than 500 °C, where methanation reactions are well known to be favored, providing evidence that hydrogen consumption is low and therefore, methanation reactions are eliminated; (c) the maximum value of S_{CH_4} is shifted toward higher temperatures using a mixture of propane/butane, indicating that the onset of methane steam reforming is delayed.

It should be noted that part of CH_4 produced, especially at low steam/C ratios under both C_3H_8 and C_3H_8/C_4H_{10} steam reforming, may be due to the decomposition of propane (Equation (8)) or butane (Equation (9)). However, no traces of C_2H_6 or C_2H_4 were detected in the results of Figure 3 and Figure S1, implying that propane or butane cracking toward smaller hydrocarbons is not operable under the present experimental conditions. In all cases examined, the carbon balance is satisfactory, with a deviation of $\approx 5\%$.

The differences discussed above can be clearly seen in Figure 5, where reactants conversion and selectivities toward reaction products at 500 and 600 °C are plotted as a function of H_2O/C ratio under conditions of both C_3H_8 (Figure 5a,b) and C_3H_8/C_4H_{10} (Figure 5c,d) steam reforming. In the absence of butane in the feed, propane conversion as well as H_2 and CO_2 selectivities increase with increasing the steam/C ratio from 2.0 to 7.0 followed by a parallel decrease of both CO and CH_4 selectivities. The extent of both conversion and selectivities variation depends on the reaction temperature. For example, the increase of $X_{C_3H_8}$ was found to be higher (from 47 to 83%) at 500 °C (Figure 5a), whereas the increase of both S_{H_2} (from 83 to 98%) and S_{CO_2} (from 34 to 72%) as well as the decrease of S_{CH_4} (from 22 to 4%) appeared to be higher at 600 °C (Figure 5b). The extent of S_{CO} decrease was similar (from ≈ 46 to 25%) at both 500 and 600 °C. The same trends were observed with respect to $X_{C_3H_8}$, $X_{C_4H_{10}}$, S_{CO_2} , and S_{CO} variations with increasing steam/C ratio in the range of 2–7 in the presence of butane in the feed (Figure 5c,d). This is also the case for variations of S_{CH_4} and S_{H_2} at 600 °C. However, a different trend was observed at 500 °C for both S_{CH_4} and S_{H_2} , which were found to be slightly increased and decreased, respectively, with increasing steam content.

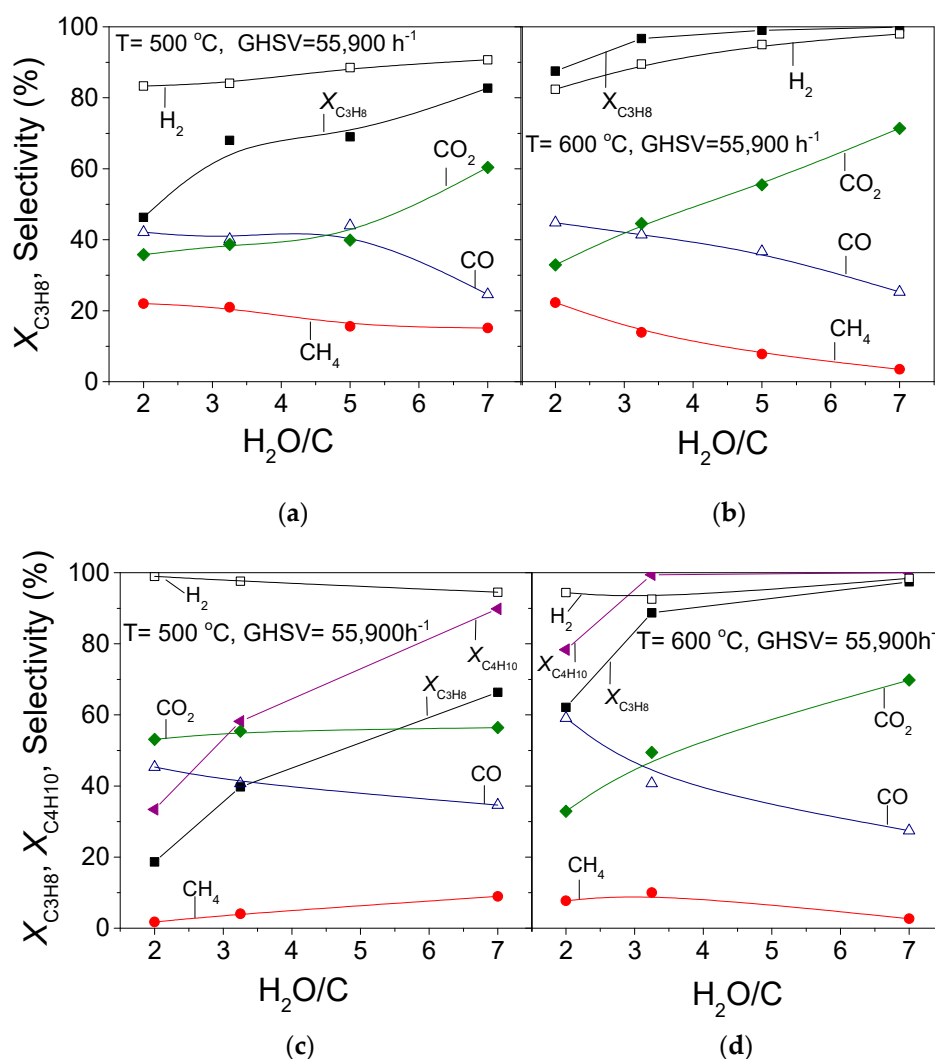


Figure 5. Effect of H_2O/C on (a,b) the conversion of C_3H_8 and selectivities toward reaction products obtained under conditions of C_3H_8 steam reforming and (c,d) the conversion of propane, conversion of butane, and selectivities toward reaction products obtained under conditions of C_3H_8/C_4H_{10} steam reforming over $0.5\%Rh/TiO_2$ at 500 and $600\text{ }^\circ\text{C}$.

The results of the present study are in excellent agreement with those reported by Laosiripojana et al. [9], who investigated the effect of inlet steam content on the LPG reforming activity over $Ni/Gd-CeO_2$ catalysts. They found that increasing the H_2O/LPG molar ratio from 1.0 to 10.0 favors the WGS reaction and therefore the production of both H_2 and CO_2 . However, the production of CO , CH_4 , C_2H_4 , and C_2H_6 was found to be eliminated due to further reforming of these compounds under conditions of excess steam. Similarly, Çağlayan et al. [34] found that H_2 production increases by 20% with increasing the steam/ C ratio from 2 to 3 over $Pt-Ni/\delta-Al_2O_3$ catalyst. Moreover, Al-Zuhair et al. [1] demonstrated that the H_2 yield and the ratio of $H_2:CH_4$ selectivity increase with increasing the steam/ C ratio from 4.5 to 6.5 over Ru/Al_2O_3 catalyst. An increase of H_2 production was also reported with increasing the steam to carbon ratio under conditions of sorption-enhanced steam reforming of propane over Ni catalyst using an in situ carbonation of CaO [35]. However, in that study, CH_4 production was found to be higher with decreasing propane content due to the increase of chemisorbed oxygen species, which are able to reform the dissociative chemisorbed propane molecules. Moreover, Kolb et al. [36] demonstrated that in the case of $Rh/Pt/CeO_2$ catalyst, $X_{C_3H_8}$ increases significantly with increasing H_2O/C ratio from 0.5 to 1.6, whereas higher values of H_2O/C have only little effect on the conversion achieved. Carbon monoxide and carbon dioxide

exhibited a maximum and a minimum selectivity, respectively, for a H_2O/C ratio equal to 0.8, whereas methane selectivity was progressively decreased with the increasing H_2O content, which is in agreement with the results of Figure 5a,b,d. Different results were reported over $La_{0.8}Sr_{0.2}Cr_{0.85}Ru_{0.15}O_3$ catalyst for which the increase of H_2O/C ratio in the range of 1–3 practically affected neither propane conversion nor product selectivities [37]. Any difference observed between the results of the present study and those reported in the literature may be attributed to the different type of catalysts and reaction conditions (e.g., temperature, W/F ratio etc.) employed.

2.3. Effect of Gas Hourly Space Velocity on Catalytic Performance

Results presented in Figures 2 and 4 were obtained with a relatively high GHSV of ca $55,900\text{ h}^{-1}$. In order to investigate the effect of GHSV on the catalytic performance for propane steam reforming reaction, experiments were conducted by varying this parameter in the range of $16,800\text{--}78,200\text{ h}^{-1}$ over $0.5\%Rh/TiO_2$ catalyst using a steam/C ratio equal to 3.25. The results obtained are shown in Figure 6, where it is observed that the conversion curve of C_3H_8 is progressively shifted toward lower temperatures (by $\approx 65\text{ }^\circ\text{C}$) with decreasing GHSV. This is due to the higher residence time achieved by decreasing the space velocity, which subsequently leads to higher propane conversion [38,39]. Interestingly, for $GHSV = 16,800\text{ h}^{-1}$, the $0.5\%Rh/TiO_2$ catalyst is able to achieve complete propane conversion at temperatures as low as $570\text{ }^\circ\text{C}$.

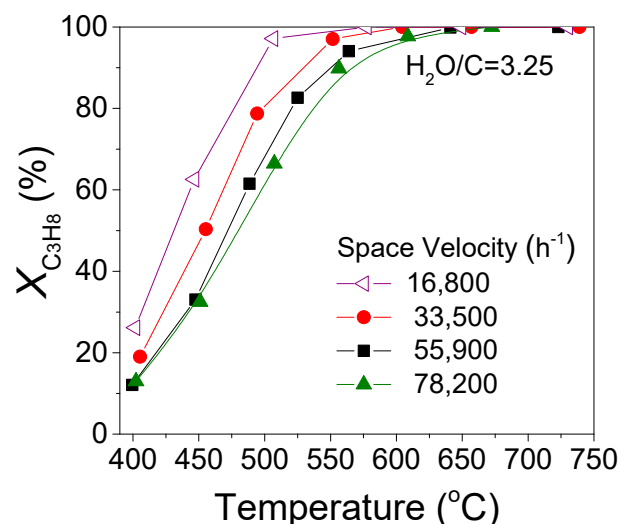


Figure 6. Effect of GHSV on the conversion of C_3H_8 obtained as a function of reaction temperature over $0.5\%Rh/TiO_2$ catalyst. Experimental conditions: $H_2O/C:3.25$; particle diameter: $0.15 < d_p < 0.25\text{ mm}$; feed composition: $4.5\% C_3H_8$, $0.15\% Ar$, $44\% H_2O$ (balance He).

Product distribution results are summarized in Figure S2. It is observed that for $GHSV = 16,800\text{--}78,200\text{ h}^{-1}$, selectivities toward CO and CO_2 do not vary significantly with temperature, ranging between 33 and 55%, and they do not present any trend with respect to GHSV. This is most probably due to the involvement of CO and CO_2 , both as reactants and products, to several reactions (CO/CO_2 hydrogenation, Reverse WGS (RWGS), propane, and methane steam reforming) running in parallel under the present conditions. The main difference observed is related to CH_4 formation, of which the maximum selectivity is gradually decreased from 36 to 25%, whereas the temperature of its appearance is shifted from 485 to 535 $^\circ\text{C}$ with increasing GHSV. This indicates that the conversion of CO/CO_2 to CH_4 at low temperatures and the CH_4 steam-reforming reaction at high temperatures are favored for low space velocities in agreement with previous studies [38,40].

The effect of GHSV on catalytic performance is less pronounced in the presence of a small concentration of butane in the feed (Figure 7). The conversion curves of both

propane and butane are only slightly shifted toward lower temperatures (by ≈ 40 °C) with decreasing GHSV from 16,800 to 78,200 h^{-1} . The effect is even less important below 480 °C, where all data points lie on the same line. A comparison of Figures 6 and 7a implies that propane steam reforming is significantly suppressed under conditions of propane/butane steam reforming. In particular, for $\text{GHSV} = 16,800 \text{ h}^{-1}$, $X_{\text{C}_3\text{H}_8}$ decreases from 94 to 45% at 500 °C and from 65 to 18% at 450 °C by adding C_4H_{10} in the gas stream. Selectivities toward reaction products are presented in Figure S3, where no significant variations are observed with respect to GHSV. Comparing Figure S3 with the results obtained in the absence of butane in the gas stream (Figure S2) indicates that the RWGS reaction predominates the CO_2 hydrogenation to CH_4 as evidenced by (a) the significant increase of S_{CO} at the expense of S_{CO_2} , (b) the suppression of CH_4 formation, and (c) the higher selectivity toward H_2 production. It should be noted that in all cases, the deviation of carbon balance was lower than 5%.

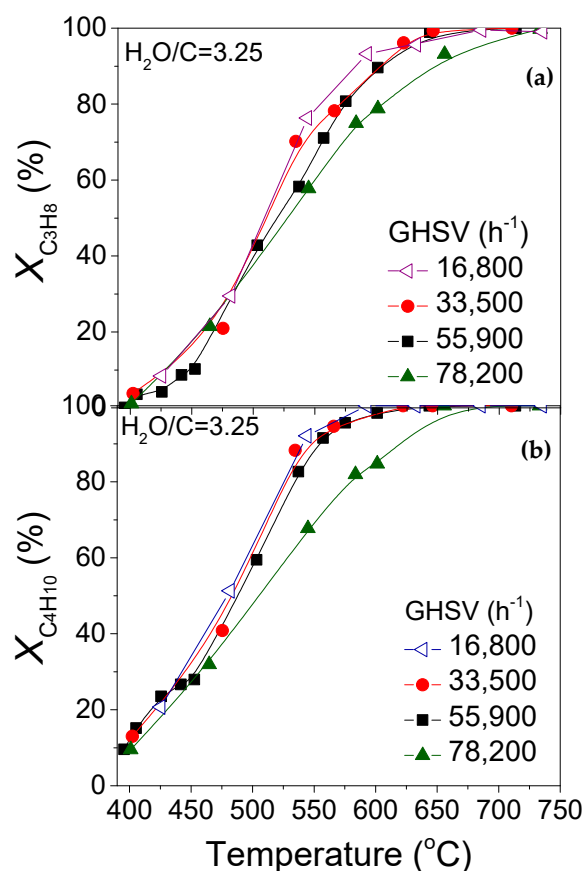


Figure 7. Effect of GHSV on the conversions of (a) C_3H_8 and (b) C_4H_{10} obtained as a function of reaction temperature over 0.5%Rh/TiO₂ catalyst. Experimental conditions: $\text{H}_2\text{O}/\text{C}=3.25$; particle diameter: $0.15 < d_p < 0.25$ mm; feed composition: 4.27% C_3H_8 , 0.23% C_4H_{10} , 0.15% Ar, 44% H_2O (balance He).

The above observations can be clearly seen in Figure 8, where $X_{\text{C}_3\text{H}_8}$, $X_{\text{C}_4\text{H}_{10}}$, and selectivities toward reaction products at 500 and 600 °C are plotted as a function of GHSV under conditions of both C_3H_8 (Figure 8a,b) and $\text{C}_3\text{H}_8/\text{C}_4\text{H}_{10}$ (Figure 8c,d) steam reforming. The trends discussed above with respect to GHSV are more pronounced at 500 °C, whereas propane and butane conversions are generally lower. In particular, under conditions of propane steam reforming, $X_{\text{C}_3\text{H}_8}$ at 500 °C decreases from 94 to 62% with increasing space velocity from 16,800 to 78,200 h^{-1} , which is followed by an increase of both S_{H_2} and S_{CO} from 73 to 82% and from 24 to 32%, respectively. The increased production of H_2 with increasing GHSV is accompanied by a decrease of S_{CH_4} (due to the suppression of CO/CO_2 methanation and enhancement of CH_4 steam reforming) from 36 to 26%, respectively. A

similar increase in H_2 selectivity was previously found with increasing space velocity for the steam reforming of a mixture of hydrocarbons (including CH_4 , C_3H_8 , C_4H_{10} , and C_2H_6) in a Pd-Au membrane reactor [38] as well as under conditions of partial oxidation of propane over bimetallic Pt-Ni/d- Al_2O_3 catalyst [34].

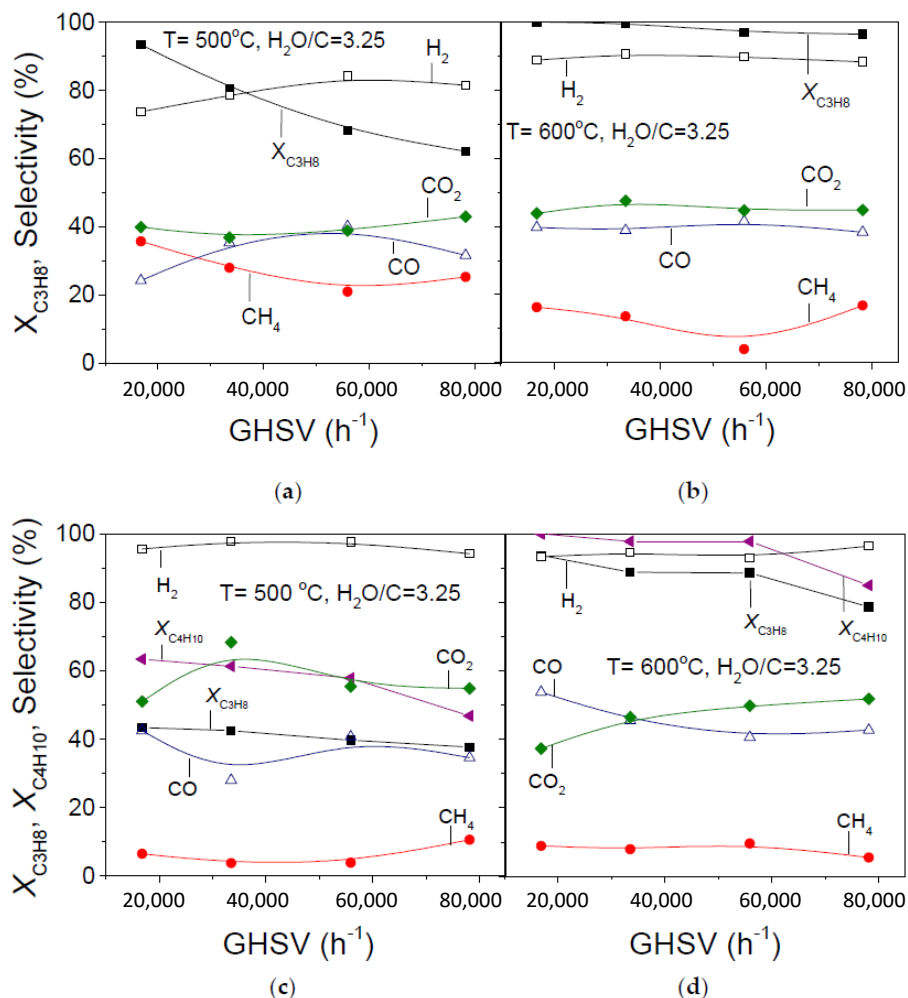


Figure 8. Effect of GHSV on (a,b) the conversion of C_3H_8 and selectivities toward reaction products obtained under conditions of C_3H_8 steam reforming and (c,d) the conversion of propane, conversion of butane, and selectivities toward reaction products obtained under conditions of C_3H_8/C_4H_{10} steam reforming over 0.5%Rh/ TiO_2 at 500 and 600 °C.

On the other hand, under conditions of propane/butane steam reforming, variations of reactants conversions and product selectivities with GHSV are less important at both temperatures investigated (Figure 8c,d). It should be noted that the effect of GHSV on catalytic performance is generally weaker than that of H_2O/C ratio both in the presence and in the absence of butane in the gas stream at least under the present experimental conditions.

2.4. Dynamic Response of Rh/ TiO_2 Catalyst to H_2O/C Ratio

The dynamic response of Rh/ TiO_2 catalyst was investigated with respect to variations of H_2O/C ratio at 550 °C under conditions of C_3H_8 steam reforming and using a $GHSV = 55,900 h^{-1}$. Results (Figure 9a) showed that neither catalytic activity nor product selectivity is varied with abrupt and successive changes of H_2O/C ratio between 2 and 7. In particular, switching the H_2O/C ratio from 7 to 2 results in a decrease of $X_{C_3H_8}$, S_{H_2} , and S_{CO_2} as well as in an increase of S_{CO} and S_{CH_4} , as it was expected according to results discussed above (Figure 2). Catalytic activity and product selectivity are completely

restored to the initial corresponding levels following the subsequent switching of H_2O/C to 7 and then to 2.

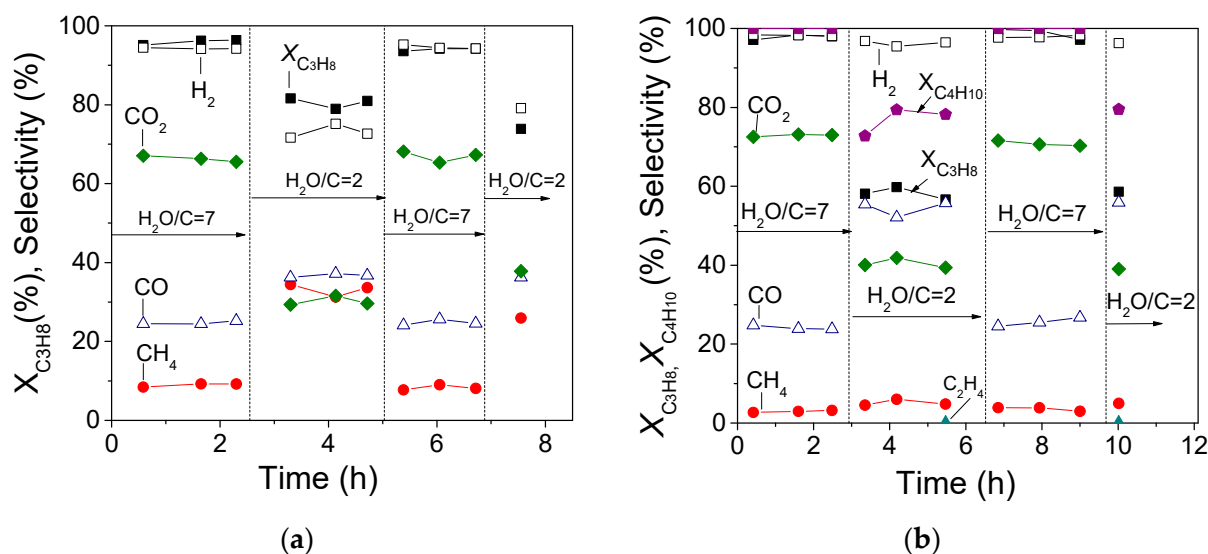


Figure 9. Dynamic response of Rh/TiO₂ catalyst to variations of H₂O/C ratio obtained (a) at 550 °C under conditions of C₃H₈ steam reforming and (b) at 600 °C under conditions of C₃H₈/C₄H₁₀ steam reforming. GHSV = 55,900 h⁻¹.

A similar experiment was conducted at 600 °C under conditions of C₃H₈/C₄H₁₀ steam reforming and using a GHSV = 55,900 h⁻¹. The selection of temperature was made so as to ensure comparable propane conversion and product selectivity with those presented in Figure 9a, and the results obtained are shown in Figure 9b. As it can be seen, $X_{C_3H_8}$, $X_{C_4H_{10}}$, and selectivities to reaction products remain constant for a period of 3 h using a steam/C ratio equal to 7. As it was expected, both reactant conversions decrease upon switching of the steam/C ratio to 2, which is accompanied by a decrease of S_{H_2} and S_{CO_2} and an increase of S_{CO} and S_{CH_4} . Traces of ethylene were also detected, indicating that propane decomposition is operable. A small scattering was observed in both conversions and product selectivities with time-on-stream, which may be due to the time required for the stabilization of feed composition following the switch of H₂O/C from 7 to 2. Subsequent switches of H₂O/C ratio to 7 and 2 result in a similar catalytic behavior. In all cases, the values of conversions and product selectivities are similar with those presented in Figure 4 for H₂O/C = 7 and 2 at 550 °C and 600 °C, respectively.

2.5. Dynamic Response of Rh/TiO₂ Catalyst to Temperature

The dynamic response of Rh/TiO₂ catalyst to temperature was investigated for the propane steam-reforming reaction over a period of 56 h on stream under the following variations of temperature: 600 °C (20 h) → 650 °C (11 h) → 500 °C (11 h) → 600 °C (14 h). The space velocity and the steam/C ratio used were equal to 55,900 h⁻¹ and 3.25, respectively. Results obtained are presented in Figure 10, where $X_{C_3H_8}$, S_{H_2} , S_{CO} , S_{CO_2} , and S_{CH_4} are plotted as functions of time-on-stream. The system was shutting down overnight (indicated by the dashed vertical lines), where the catalyst was maintained at 25 °C in He flow. It is observed that propane conversion progressively decreases from 99 to 81% during the first 9 h on stream, which is accompanied by an increase of S_{H_2} (from 92 to 96%) and S_{CO} (from 39 to 49%) and by a decrease of S_{CH_4} (from 10 to 7%) and S_{CO_2} (from 51 to 44%). Interestingly, shutting down of the system overnight in He flow resulted in recovery of both the activity and selectivities toward reaction products, which, however, followed a similar trend (decrease of $X_{C_3H_8}$, S_{CH_4} , and S_{CO_2} and increase of S_{H_2} , S_{CO}) with time-on-stream upon two subsequent cycles of exposure to reaction mixture → shutting down of the system overnight in He flow. Then, the temperature was increased at 650 °C and a propane steam-reforming reaction was conducted for a period of 11 h. As it can be

seen in Figure 10, both propane conversion and product selectivities remain constant with time. This is also the case for the activity and selectivity of Rh/TiO₂ catalyst following a subsequent decrease of temperature at 500 °C and remaining at this temperature for 11 h on stream (Figure 10). However, when the reaction temperature increases again at 600 °C, a similar behavior was observed to that discussed above during the first 20 h; i.e., a temporary catalyst deactivation and variation in products distribution was observed, whereas a switch of the reaction mixture to He flow leads to a recovery of initial activity and product selectivity. Then, the catalyst was progressively deactivated upon a subsequent exposure to the reaction mixture. It should be noted that the deviation of carbon balance during the stability test ranged between 5 and 10%, which as it will be discussed below may be related to the small amount of carbon accumulated on the catalyst surface under reaction conditions.

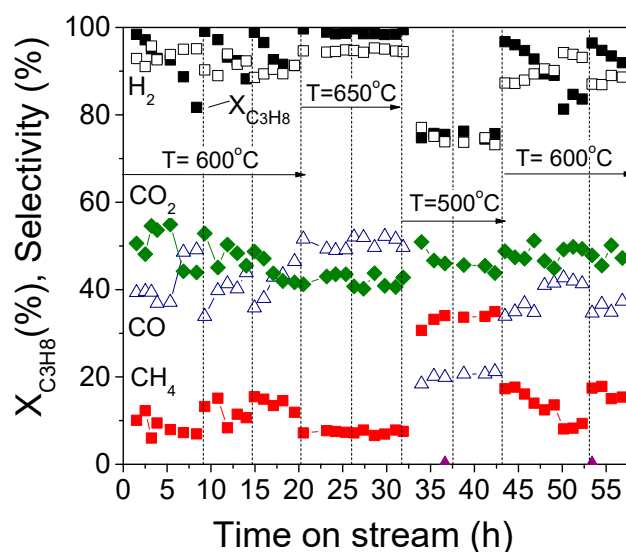


Figure 10. Long-term stability test of the 0.5%Rh/TiO₂ catalyst under conditions of C₃H₈ steam reforming: Alterations of the conversion of C₃H₈ and selectivities toward reaction products with time-on-stream. Experimental conditions: H₂O/C = 3.25; GHSV = 55,900 h⁻¹; T = 500, 600, and 650 °C.

Taking into account that both the conversion and selectivity of reaction products remain constant with time when the reaction takes place at 650 and 500 °C, it can be suggested that a possible step inducing a reversible catalyst deactivation occurs at 600 °C, leading to the behavior discussed above. In order to further investigate this, the spent catalyst (denoted as Rh/TiO₂-56h) after the stability test presented in Figure 10 was characterized employing BET and XRD techniques. Moreover, a Temperature-Programmed Oxidation (TPO) experiment was performed over the spent catalyst in order to check for possible carbon deposition. The results of BET measurements showed that the specific surface area of the Rh/TiO₂ catalyst decreases significantly, from 43 to 6.6 m²/g, after 56 h-on-stream (Table 1). This may be due (a) to the high temperatures (500–650 °C) where the long-term stability test was performed, which are well known to induce a decrease of SSA and/or (b) to the steam-reforming chemistry [41,42]. The increase of temperature above 600 °C may be also responsible for the complete transformation of anatase to rutile phase of TiO₂ support, as evidenced by XRD patterns obtained for the spent Rh/TiO₂-56h sample (Figure 1, trace c) [41,43,44]. Apart from the reflections attributed to the rutile phase of TiO₂, an additional peak located at 72.4° can be hardly discerned in the XRD diffractogram of the Rh/TiO₂-56h sample. This peak has been previously assigned to graphite carbon [45,46], which, as it will be discussed below, is deposited on the catalyst surface under reaction conditions. The exposure of Rh/TiO₂ catalyst to the reformat mixture for 56 h also resulted in a significant increase of TiO₂ crystallite size from 34.0 to 49.6 nm (Table 1). In order to clarify whether the increase of *d*_{TiO₂} and the decrease of SSA were due to the high temperature where the sta-

bility test was conducted and/or to the steam-reforming chemistry, a Rh/TiO₂ catalyst was prepared that was calcined in air at 600 °C for 3 h (denoted as Rh/TiO₂-600 °C) followed by H₂ reduction at 300 °C. Heat treatment of the catalyst at 600 °C resulted in a decrease of SSA from 43 to 30 m²/g and an increase of rutile content from 17.3 to 41% (Table 1, Figure 1 (trace b)). However, the crystallite size of TiO₂ was not practically changed, taking values of 23 and 35 nm for the anatase and rutile phase, respectively. The results of Table 1 imply that the physicochemical properties of TiO₂ are not dramatically varied upon calcination at 600 °C. Although the spent Rh/TiO₂-56h catalyst was exposed to 600 °C for a significantly longer time compared to the fresh Rh/TiO₂-600 °C sample, the steam-reforming chemistry seems to contribute to the variations of its physicochemical characteristics. In any case, the observed decrease of propane conversion with time-on-stream at 600 °C (Figure 10) should not be related to the variations of SSA and d_{TiO_2} discussed above, since $X_{\text{C}_3\text{H}_8}$ and product selectivities are completely restored upon catalyst exposure to He flow.

In order to further investigate the effect of variations of the physicochemical properties of catalyst on its performance with time-on-stream, a stability test of fresh Rh/TiO₂ catalyst for a propane steam-reforming reaction was also conducted at 650 °C for 14 h, and the spent catalyst was characterized employing BET and XRD techniques. The catalyst exhibited excellent stability with time-on-stream [29]. Characterization of the spent sample showed that the interaction of catalyst with the propane steam-reforming mixture at 650 °C for 14 h resulted in a decrease of its SSA from 43 to 9.6 m²/g, a complete transformation of the anatase phase of TiO₂ support to rutile, and an increase of the primary TiO₂ crystallite size from 34 to 54.1 nm. These variations are similar to those found for the spent catalyst after the stability test at 600 °C (Table 1), where propane conversion decreases with time-on-stream (Figure 10). This indicates that the temporary deactivation at 600 °C should not be related to the variations of physicochemical properties of catalysts discussed above, since similar variations were observed whether $X_{\text{C}_3\text{H}_8}$ decreases with time-on-stream or not. Moreover, if the catalyst deactivation at 600 °C was related to variations of its structural characteristics (e.g., Rh particle size), this deactivation was expected to be permanent, whereas $X_{\text{C}_3\text{H}_8}$ and product selectivities were not expected to be completely restored upon catalyst exposure to He flow, as observed in Figure 10. This enhances our suggestion that a possible step inducing a reversible catalyst deactivation occurs at 600 °C, leading to the behavior discussed above.

After the completion of the stability test presented in Figure 10, the catalyst was cooled to room temperature under He flow, and a TPO experiment was carried out by switching the feed composition from He to 3%O₂/He (30 cm³/min), left at 25 °C for 10 min, and then heating linearly ($\beta = 30$ °C/min) at 700 °C. The effluent gas composition was on-line monitored using an Omnistar/Pfeiffer Vacuum mass spectrometer (MS) [47]. Results of the TPO experiment are presented in Figure 11, where it is observed that the profile of CO₂ thus produced exhibits one main peak with a maximum at 330 °C followed by a shoulder at about 460 °C, indicating that there are two distinct carbon species on the catalyst surface. The amount of CO₂ produced during TPO was estimated to be 19.3 $\mu\text{mol/g}_{\text{cat}}$.

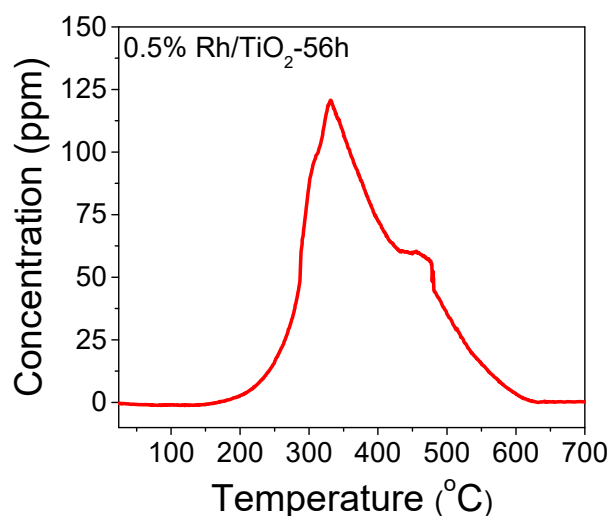


Figure 11. Responses of CO_2 produced during temperature-programmed oxidation with 3% O_2 (in He) occurred after the stability test of Figure 10 conducted over Rh/TiO₂ catalyst.

As discussed above, the origin of carbon formation may be due to the decomposition of C_2H_6 , C_2H_4 , CH_4 , and/or CO (Equations (10)–(13)). However, taking into account that no ethylene or ethane is produced under the present reaction conditions, carbon deposition due to the decomposition of those species can be excluded. This is also the case for the “Boudouard” reaction (Equation (13)), as evidenced by the increase of S_{CO} and the decrease of S_{CO_2} with time-on-stream at 600 °C, which accompany the progressive decrease of $X_{\text{C}_3\text{H}_8}$. Moreover, the latter reaction is thermodynamically favored at significantly lower temperatures (<400 °C). Therefore, CH_4 decomposition (Equation (13)) is the main contributor to carbon species, which is also supported by the progressive decrease of S_{CH_4} followed by the increase of S_{H_2} [48–51].

The recovery of catalytic activity upon switching the reaction mixture to He flow at 600 °C as well as the retention of $X_{\text{C}_3\text{H}_8}$ with time-on-stream at higher (650 °C) temperatures can be attributed to coke gasification and/or hydrogenation, which seems to be facilitated under conditions where CH_4 decomposition is suppressed. It can be suggested that carbon formation may not be operable at temperatures lower than 600 °C (e.g., 500 °C), whereas at higher temperatures, the carbon removal rate may be higher than the carbon formation rate, thus resulting in a no-net carbon accumulation on the catalyst surface and consequently in the observed stable performance with time-on-stream [52]. Faria et al. [2] also proposed that carbon deposition depends on the balance between the rate of CH_x species formation and the rate of carbon removal. Since CH_x species are methane precursors and methane formation is suppressed above 600 °C, it may be reasonable to suggest that the rate of methane decomposition will be lower at higher temperatures at least than the rate of carbon removal from the catalyst surface. Moreover, it has been proposed that for catalysts supported on reducible metal oxides, such as TiO₂, carbon may react with the lattice oxygen of the support, resulting in CO production and thus removing carbon from the catalyst surface [2,22]. The lattice oxygen of reducible metal oxides has been also reported to oxidize gaseous hydrocarbons, such as methane. This process is favored at high temperatures, inhibiting carbon deposition via hydrocarbons decomposition [22], and it may be the case for the excellent stability of Rh/TiO₂ at 650 °C (Figure 10).

2.6. Catalytic Performance and Long-Term Stability Test of Rh/TiO₂ Catalyst under Realistic Reaction Conditions

In order to investigate the catalytic performance of 0.5%Rh/TiO₂ catalyst under realistic reaction conditions, we prepared a catalyst in the form of 1/16-inch pellets and tested using a feed stream consisting of 4.27% C_3H_8 , 0.23% C_4H_{10} , 0.15% Ar, 44% H_2O (balance He), and a space velocity of 9000 h⁻¹. The results obtained are presented in

Figure 12, where the conversions of reactants (Figure 12a) and selectivities toward reaction products (Figure 12b) are plotted as a function of reaction temperature. It is observed that the 0.5%Rh/TiO₂ catalyst is able to achieve conversions of both propane and butane higher than 90% above 500 and 465 °C, respectively. The product distribution results demonstrated that temperatures lower than 450 °C favor CO₂ methanation reaction, whereas the RWGS as well as propane, butane, and methane steam reforming are enhanced at higher temperatures. Traces of ethylene and ethane were also detected at low temperatures, indicating that propane and butane decomposition (Equations (8) and (9)) take place, contributing to a small extent to CH₄ production below 450 °C.

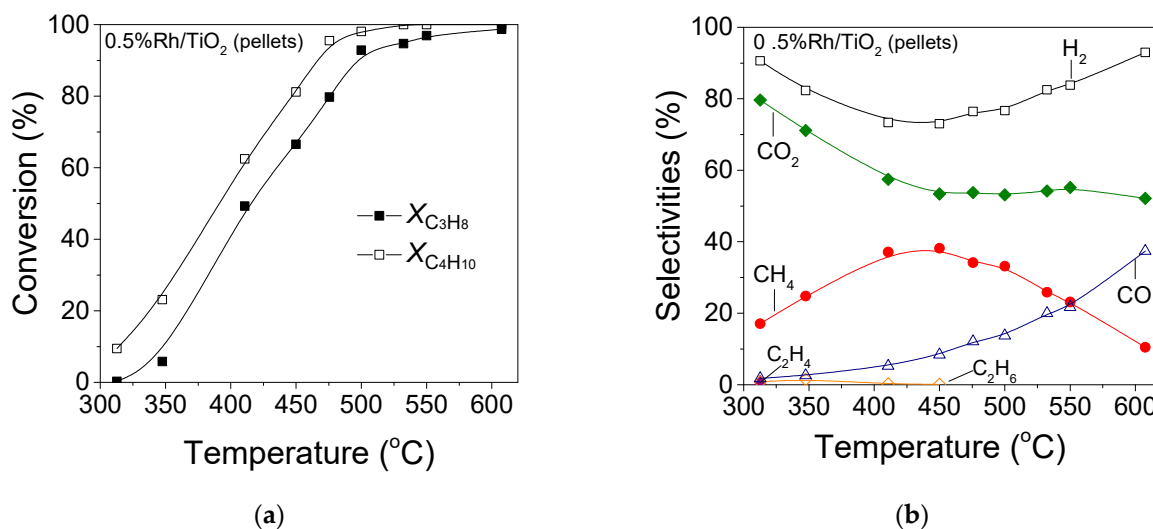


Figure 12. Catalytic performance of 0.5%Rh/TiO₂ catalyst in the form of pellets for the propane/butane steam-reforming reaction under realistic reaction conditions. (a) Conversions of C₃H₈ and C₄H₁₀; (b) Selectivities toward reaction products. Experimental conditions: H₂O/C = 3.25; GHSV = 9000 h⁻¹; Feed composition: 4.27% C₃H₈, 0.23% C₄H₁₀, 0.15% Ar, 44% H₂O.

The long-term stability of 0.5%Rh/TiO₂ pellets was investigated at 550 and 500 °C using the same experimental conditions with those used in Figure 12. It was found that 0.5%Rh/TiO₂ exhibits excellent stability at 550 °C for about 12 h-on-stream, with the conversions of propane and butane being about 98% and 99%, respectively (Figure 13). Product selectivity also remained stable, taking values of S_{H₂} = 83–84%, S_{CH₄} = 23–24%, S_{CO₂} = 53–55%, and S_{CO} = 19–21%. A decrease of temperature at 500 °C results in a decrease of X_{C₃H₈} and X_{C₄H₁₀} to 93 and 98%, respectively. Interestingly, both conversions are gradually increased with time-on-stream, reaching the values of 98% (for C₃H₈) and 100% (for C₄H₁₀), which remain constant for about 18 h-on-stream.

Hydrogen selectivity decreases to 70–72% with decreasing temperature to 500 °C, which is followed by an increase of S_{CH₄} (37–39%) and a decrease of S_{CO} (9–10%), whereas S_{CO₂} remains practically unaffected (51–54%). These variations can be attributed to the enhancement of CO/CO₂ methanation reactions at lower temperatures at the expense of the RWGS reaction, resulting in lower CO production, higher CH₄ formation, as well as higher H₂ consumption in accordance with the methanation reaction stoichiometry. The results of Figure 13 clearly demonstrated that both reactants conversion and product selectivity of 0.5%Rh/TiO₂ pellets remained constant at both temperatures under realistic reaction conditions for a total period of 30 h-on-stream.

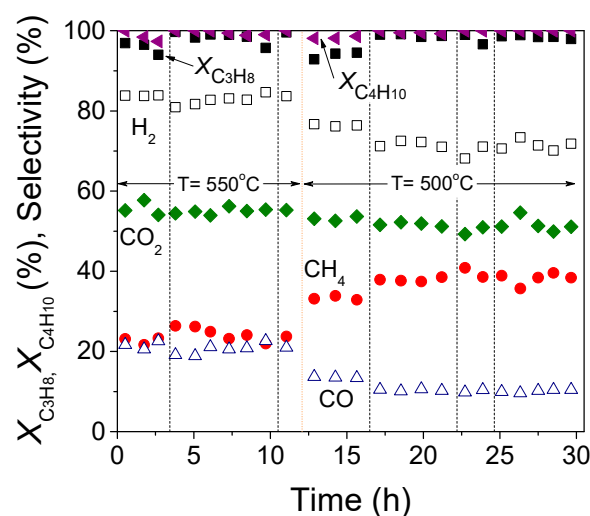


Figure 13. Long-term stability test of 0.5%Rh/TiO₂ catalyst in the form of pellets at T = 550 and 500 °C: Alterations of the conversion of C₃H₈ and C₄H₁₀, and selectivities toward reaction products with time-on-stream. Experimental conditions: Same as in Figure 12. Dashed vertical black lines indicate shutting down of the system overnight. Dashed vertical red line indicates switch of temperature from 550 to 500 °C.

3. Materials and Methods

3.1. Catalyst Preparation and Characterization

The Rh/TiO₂ catalyst was prepared employing the wet impregnation method with the use of TiO₂ (Aeroxide P25, Evonik Industries AG, Essen, Germany) powder as support and Rh(NO₃)₃ (Alfa) as the rhodium precursor salt [29]. The nominal Rh loading of the catalyst thus prepared was 0.5 wt.%. The same catalyst was also synthesized in the form of 1/16-inch pellets by impregnating TiO₂ pellets (Aerolyst) with Rh(NO₃)₃ (Alfa), where the excess of water was gradually removed by a rotary evaporator at 70 °C. The TiO₂ (Aerolyst) was commercially available (Evonik Industries AG, Essen, Germany) in the form of 1/16-inch pellets. In both cases, the impregnation is followed by drying at 110 °C overnight and a reduction at 300 °C in H₂ flow for 2 h.

The specific surface area (BET) of Rh/TiO₂ catalyst was estimated by N₂ physical adsorption (77 K), whereas the phase composition and crystallite size of TiO₂ were determined employing the XRD technique. Hydrogen chemisorption measurement was also conducted for the estimation of Rh dispersion and mean particle size. Details on the apparatus and procedures used have been described in detail in the Supplementary Material.

3.2. Catalytic Performance Tests

Catalytic performance tests were carried out in the temperature range of 400–750 °C using an apparatus, which has been described in our previous study [29]. The GHSV was varied in the range of 16,800–78,200 h⁻¹. In a typical experiment, the catalyst was placed in a quartz microreactor, heated at 300 °C under He flow, and then reduced in situ at 300 °C for 1 h under 50%H₂/He flow (60 cm³ min⁻¹). Then, the temperature was increased at 750 °C under He, and then the sample was exposed to the reaction mixture consisting of 4.5%C₃H₈ + 0.15%Ar + 44%H₂O (He balance). Then, measurements were obtained by the stepwise decreasing temperature. The catalyst remained at each temperature for 1 h. A number of experiments were also carried out in the presence of 0.23% butane (C₃H₈:C₄H₁₀ = 95:5) in the gas stream. Separate experiments were also performed to examine the influence of H₂O/C molar ratio on catalytic activity by varying this parameter from 2 to 7. The conversion of reactants and selectivities toward products were determined at steady-state conditions using two gas chromatographs (Shimadzu, Kyoto, Japan) connected in parallel through a common set of switch valves and employing

the procedures described elsewhere [29]. Argon was used as internal standard in order to account for the volume change.

The conversions of propane ($X_{C_3H_8}$) and butane ($X_{C_4H_{10}}$) were calculated using the following expressions.

$$X_{C_3H_8} = \frac{[C_3H_8]_{in} - [C_3H_8]_{out}}{[C_3H_8]_{in}} \times 100 \quad (14)$$

$$X_{C_4H_{10}} = \frac{[C_4H_{10}]_{in} - [C_4H_{10}]_{out}}{[C_4H_{10}]_{in}} \times 100 \quad (15)$$

Selectivity toward reaction products containing carbon was defined using the following equation, where the factor n corresponds to the number of carbon atoms in the corresponding molecule (e.g., for CO, it is 1, for C_2H_4 , it is 2, etc.).

$$S_{C_n} = \frac{[C_n] \times n}{[CO] + [CO_2] + [CH_4] + 2 \times ([C_2H_4] + [C_2H_6]) + 3 \times [C_3H_6]} \times 100 \quad (16)$$

Hydrogen selectivity was estimated by Equation (17) where the factor m represents the number of hydrogen atoms in the corresponding molecule (e.g., for CH_4 and C_2H_4 , it is 4).

$$S_{H_2}(\%) = \frac{[H_2]}{[H_2] + m/2 \times [C_nH_m]} \times 100 \quad (17)$$

The overall carbon balance of the catalytic performance experiments was calculated using Equation (18).

$$[Carbon]_{total,out} = \frac{[CO] + [CO_2] + [CH_4]}{3} + 2 \times \frac{[C_2H_4] + [C_2H_6]}{3} \quad (18)$$

4. Conclusions

The results of the present study showed that Rh/TiO₂ catalyst is capable of selectively producing H₂ via LPG steam reforming, provided that the operating reaction conditions are properly selected. Catalytic performance is enhanced with decreasing GHSV and/or increasing steam/C molar ratio. The decrease of GHSV does not affect appreciably product selectivities. In contrast, increase of the H₂O concentration in the feed significantly affects product distribution favoring propane steam reforming and WGS and suppressing methanation reactions. The effect of steam/C ratio on catalytic performance was found to be higher under conditions of propane steam reforming than that observed under conditions of propane/butane steam reforming, while the opposite was found for the effect of GHSV. The propane steam-reforming reaction is generally suppressed in the presence of butane in the gas stream, resulting in lower propane conversions. Moreover, the RWGS reaction predominates the CO₂ hydrogenation to CH₄ when propane and butane coexist in the reaction mixture. The titania-supported Rh catalyst exhibits excellent stability and high durability of operating condition fluctuation at temperatures of practical interest, and therefore, it is promising for the production of H₂ via LPG steam reforming for fuel cell applications.

Supplementary Materials: The following are available online at <https://www.mdpi.com/2073-4344/11/3/374/s1>, Materials characterization methods; Experimental set-up for catalytic performance tests; Scheme S1: Experimental set-up for catalytic performance tests; Figure S1: Effect of H₂O/C ratio on the selectivities toward reaction products obtained as function of reaction temperature over 0.5%Rh/TiO₂ catalyst. Experimental conditions: GHSV: 55,900 h⁻¹; particle diameter: 0.15 < d_p < 0.25 mm; Feed composition: 2.0–5.7% C₃H₈, 0.1–0.3% C₄H₁₀, 0.15–0.20% Ar, 36.8–44.1% H₂O (balance He); Figure S2: Effect of GHSV on the selectivities toward reaction products obtained as a function of reaction temperature over 0.5%Rh/TiO₂ catalyst. Experimental conditions: Steam/C: 3.25; particle diameter: 0.15 < d_p < 0.25 mm; Feed composition: 4.5% C₃H₈, 0.15% Ar, 44% H₂O (balance He); Figure S3: Effect of GHSV on the selectivities toward reaction products obtained as

function of reaction temperature over 0.5%Rh/TiO₂ catalyst. Experimental conditions: Steam/C: 3.25; particle diameter: 0.15 < d_p < 0.25 mm; Feed composition: 4.27% C₃H₈, 0.23% C₄H₁₀, 0.15% Ar, 44% H₂O (balance He).

Author Contributions: Conceptualization, P.P.; methodology, P.P.; investigation, A.K., T.R. and P.P.; data curation, A.K., T.R. and P.P.; writing—original draft preparation, P.P.; writing—review and editing, P.P.; visualization, P.P.; supervision, P.P.; project administration, P.P.; funding acquisition, P.P. All authors have read and agreed to the published version of the manuscript.

Funding: This research has been co-financed by the European Union and Greek national funds through the Operational Program Competitiveness, Entrepreneurship and Innovation, under the call RESEARCH—CREATE—INNOVATE (project code:T1EDK-02442).

Conflicts of Interest: The authors declare no conflict of interest. The funders had no role in the design of the study; in the collection, analyses, or interpretation of data; in the writing of the manuscript, or in the decision to publish the results.

References

1. Al-Zuhair, S.; Hassan, M.; Djama, M.; Khaleel, A. Hydrogen Production by Steam Reforming of Commercially Available LPG in UAE. *Chem. Eng. Commun.* **2016**, *204*, 141–148. [[CrossRef](#)]
2. Faria, E.C.; Rabelo-Neto, R.C.; Colman, R.C.; Ferreira, R.A.R.; Hori, C.E.; Noronha, F.B. Steam Reforming of LPG over Ni/Al₂O₃ and Ni/Ce_xZr_{1-x}O₂/Al₂O₃ Catalysts. *Catal. Lett.* **2016**, *146*, 2229–2241. [[CrossRef](#)]
3. Ipsakis, D.; Papadopoulou, S.; Voutetakis, S.; Seferlis, P. Analysis and Implementation of a Plant-Wide Control System for an LPG Reforming-Fuel Cell Power System. In *Chemical Engineering Transactions*; AIDIC Servizi S.r.l.: Milan, Italy, 2013; Volume 35, pp. 955–960.
4. Panagiotopoulou, P.; Papadopoulou, C.; Matralis, H.; Verykios, X. Production of Renewable Hydrogen by Reformation of Biofuels. In *Advances in Bioenergy: The Sustainability Challenge*; Wiley: Hoboken, NJ, USA, 2015; pp. 109–130. [[CrossRef](#)]
5. Ligras, D.K.; Kondarides, D.I.; Verykios, X.E. Production of hydrogen for fuel cells by steam reforming of ethanol over supported noble metal catalysts. *Appl. Catal. B Environ.* **2003**, *43*, 345–354. [[CrossRef](#)]
6. Silva, P.P.; Ferreira, R.A.; Noronha, F.B.; Hori, C.E. Hydrogen production from steam and oxidative steam reforming of liquefied petroleum gas over cerium and strontium doped LaNiO₃ catalysts. *Catal. Today* **2017**, *289*, 211–221. [[CrossRef](#)]
7. Wang, G.; Yu, Y.; Liu, H.; Gong, C.; Wen, S.; Wang, X.; Tu, Z. Progress on design and development of polymer electrolyte membrane fuel cell systems for vehicle applications: A review. *Fuel Process. Technol.* **2018**, *179*, 203–228. [[CrossRef](#)]
8. Kolb, G.; Keller, S.; O'Connell, M.; Pecov, S.; Schuerer, J.; Spasova, B.; Tiemann, D.; Ziogas, A. Microchannel Fuel Processors as a Hydrogen Source for Fuel Cells in Distributed Energy Supply Systems. *Energy Fuels* **2013**, *27*, 4395–4402. [[CrossRef](#)]
9. Laosiripojana, N.; Sutthisripok, W.; Charojrochkul, S.; Assabumrungrat, S. Steam reforming of LPG over Ni and Rh supported on Gd-CeO₂ and Al₂O₃: Effect of support and feed composition. *Fuel* **2011**, *90*, 136–141. [[CrossRef](#)]
10. Afolabi, A.T.F.; Kechagiopoulos, P.N.; Liu, Y.; Li, C.-Z. Kinetic features of ethanol steam reforming and decomposition using a biochar-supported Ni catalyst. *Fuel Process. Technol.* **2021**, *212*, 106622. [[CrossRef](#)]
11. Huang, T.-J.; Wu, C.-Y.; Wang, C.-H. Fuel processing in direct propane solid oxide fuel cell and carbon dioxide reforming of propane over Ni-YSZ. *Fuel Process. Technol.* **2011**, *92*, 1611–1616. [[CrossRef](#)]
12. Remón, J.; Jarauta-Córdoba, C.; García, L.; Arauzo, J. Analysis and optimisation of H₂ production from crude glycerol by steam reforming using a novel two step process. *Fuel Process. Technol.* **2016**, *145*, 130–147. [[CrossRef](#)]
13. Haryanto, A.; Fernando, S.; Murali, N.; Adhikari, S. Current Status of Hydrogen Production Techniques by Steam Reforming of Ethanol: A Review. *Energy Fuels* **2005**, *19*, 2098–2106. [[CrossRef](#)]
14. Douette, A.M.D.; Turn, S.Q.; Wang, W.; Keffer, V.I. Experimental Investigation of Hydrogen Production from Glycerin Reforming. *Energy Fuels* **2007**, *21*, 3499–3504. [[CrossRef](#)]
15. Tang, R.; Tian, Y.; Qiao, Y.; Zhao, G.; Zhou, H. Light Products and H₂-Rich Syngas over the Bifunctional Base Catalyst Derived from Petroleum Residue Cracking Gasification. *Energy Fuels* **2016**, *30*, 8855–8862. [[CrossRef](#)]
16. Recupero, V.; Pino, L.; Vita, A.; Cipiti, F.; Cordaro, M.; Laganà, M. Development of a LPG fuel processor for PEFC systems: Laboratory scale evaluation of autothermal reforming and preferential oxidation subunits. *Int. J. Hydrog. Energy* **2005**, *30*, 963–971. [[CrossRef](#)]
17. Borges, R.P.; Moura, L.G.; Spivey, J.J.; Noronha, F.B.; Hori, C.E. Hydrogen production by steam reforming of LPG using supported perovskite type precursors. *Int. J. Hydrog. Energy* **2020**, *45*, 21166–21177. [[CrossRef](#)]
18. Rakib, M.A.; Grace, J.R.; Lim, C.J.; Elnashaie, S.S.E.H.; Ghiasi, B. Steam reforming of propane in a fluidized bed membrane reactor for hydrogen production. *Int. J. Hydrog. Energy* **2010**, *35*, 6276–6290. [[CrossRef](#)]
19. Ahmed, K.; Gamman, J.; Föger, K. Demonstration of LPG-fueled solid oxide fuel cell systems. *Solid State Ion.* **2002**, *152*, 485–492. [[CrossRef](#)]
20. Moura, L.G.; Borges, R.P.; Noronha, F.B.; Hori, C.E. Steam reforming of liquefied petroleum gas using catalysts supported on ceria-silica. *Int. J. Hydrog. Energy* **2020**, *46*, 1801–1814. [[CrossRef](#)]

21. Im, Y.; Lee, J.H.; Kwak, B.S.; Do, J.Y.; Kang, M. Effective hydrogen production from propane steam reforming using M/NiO/YSZ catalysts (M = Ru, Rh, Pd, and Ag). *Catal. Today* **2018**, *303*, 168–176. [[CrossRef](#)]
22. Laosiripojana, N.; Assabumrungrat, S. Hydrogen production from steam and autothermal reforming of LPG over high surface area ceria. *J. Power Sources* **2006**, *158*, 1348–1357. [[CrossRef](#)]
23. Gökaliler, F.; Selen Çağlayan, B.; Ilsen Önsan, Z.; Erhan Aksoylu, A. Hydrogen production by autothermal reforming of LPG for PEM fuel cell applications. *Int. J. Hydrog. Energy* **2008**, *33*, 1383–1391. [[CrossRef](#)]
24. Fard, A.A.; Arvaneh, R.; Alavi, S.M.; Bazyari, A.; Valaei, A. Propane steam reforming over promoted Ni—Ce/MgAl₂O₄ catalysts: Effects of Ce promoter on the catalyst performance using developed CCD model. *Int. J. Hydrog. Energy* **2019**, *44*, 21607–21622. [[CrossRef](#)]
25. Fard, A.A.; Bazyari, A.; Alavi, S.M.; Aghamiri, A.R. The effects of cobalt and cerium promoters on hydrogen production performance of alumina-supported nickel catalysts in propane steam reforming. *J. Chem. Technol. Biotechnol.* **2020**, *95*, 3241–3251. [[CrossRef](#)]
26. Shoynkhorova, T.B.; Rogozhnikov, V.N.; Ruban, N.V.; Shilov, V.A.; Potemkin, D.I.; Simonov, P.A.; Belyaev, V.D.; Snytnikov, P.V.; Sobyenin, V.A. Composite Rh/Zr_{0.25}Ce_{0.75}O_{2-δ}-γ-Al₂O₃/Fecralloy wire mesh honeycomb module for natural gas, LPG and diesel catalytic conversion to syngas. *Int. J. Hydrog. Energy* **2019**, *44*, 9941–9948. [[CrossRef](#)]
27. Yu, L.; Sato, K.; Nagaoka, K. Rh/Ce_{0.25}Zr_{0.75}O₂ Catalyst for Steam Reforming of Propane at Low Temperature. *ChemCatChem* **2019**, *11*, 1472–1479. [[CrossRef](#)]
28. Yu, L.; Sato, K.; Toriyama, T.; Yamamoto, T.; Matsumura, S.; Nagaoka, K. Influence of the Crystal Structure of Titanium Oxide on the Catalytic Activity of Rh/TiO₂ in Steam Reforming of Propane at Low Temperature. *Chem. A Eur. J.* **2018**, *24*, 8742–8746. [[CrossRef](#)]
29. Kokka, A.; Katsoni, A.; Yentekakis, I.V.; Panagiotopoulou, P. Hydrogen production via steam reforming of propane over supported metal catalysts. *Int. J. Hydrog. Energy* **2020**, *45*, 14849–14866. [[CrossRef](#)]
30. Chein, R.-Y.; Yu, C.-T. Thermodynamic equilibrium analysis of water-gas shift reaction using syngases-effect of CO₂ and H₂S contents. *Energy* **2017**, *141*, 1004–1018. [[CrossRef](#)]
31. Hou, T.; Yu, B.; Zhang, S.; Zhang, J.; Wang, D.; Xu, T.; Cui, L.; Cai, W. Hydrogen production from propane steam reforming over Ir/Ce_{0.75}Zr_{0.25}O₂ catalyst. *Appl. Catal. B Environ.* **2015**, *168*, 524–530. [[CrossRef](#)]
32. Tabrizi, F.F.; Mousavi, S.A.H.S.; Atashi, H. Thermodynamic analysis of steam reforming of methane with statistical approaches. *Energy Convers. Manag.* **2015**, *103*, 1065–1077. [[CrossRef](#)]
33. Wang, X.; Wang, N.; Zhao, J.; Wang, L. Thermodynamic analysis of propane dry and steam reforming for synthesis gas or hydrogen production. *Int. J. Hydrog. Energy* **2010**, *35*, 12800–12807. [[CrossRef](#)]
34. Çağlayan, B.S.; Avci, A.K.; Önsan, Z.L.; Aksoylu, A.E. Production of hydrogen over bimetallic Pt—Ni/δ-Al₂O₃: I. Indirect partial oxidation of propane. *Appl. Catal. A Gen.* **2005**, *280*, 181–188. [[CrossRef](#)]
35. Burra, K.G.; Gupta, A.K. Sorption Enhanced Steam Reforming of Propane Using Calcium Looping. In Proceedings of the ASME 2017 Power Conference Joint with ICOPE-17 collocated with the ASME 2017 11th International Conference on Energy Sustainability, the ASME 2017 15th International Conference on Fuel Cell Science, Engineering and Technology, and the ASME 2017 Nuclear Forum, Charlotte, NC, USA, 26–30 June 2017.
36. Kolb, G.; Zapf, R.; Hessel, V.; Löwe, H. Propane steam reforming in micro-channels—Results from catalyst screening and optimisation. *Appl. Catal. A Gen.* **2004**, *277*, 155–166. [[CrossRef](#)]
37. Kim, N.H.; Park, Y.-K.; Sohn, J.M. The promotion effect of catalytic activity by Ru substitution at the B site of La_{1-x}Sr_xCr_{1-y}Ru_yO_{3-z} for propane steam reforming. *Res. Chem. Intermed.* **2011**, *37*, 1313. [[CrossRef](#)]
38. Anzelmo, B.; Wilcox, J.; Liguori, S. Hydrogen production via natural gas steam reforming in a Pd-Au membrane reactor. Investigation of reaction temperature and GHSV effects and long-term stability. *J. Membr. Sci.* **2018**, *565*, 25–32. [[CrossRef](#)]
39. Park, K.S.; Son, M.; Park, M.-J.; Kim, D.H.; Kim, J.H.; Park, S.H.; Choi, J.-H.; Bae, J.W. Adjusted interactions of nickel nanoparticles with cobalt-modified MgAl₂O₄-SiC for an enhanced catalytic stability during steam reforming of propane. *Appl. Catal. A Gen.* **2018**, *549*, 117–133. [[CrossRef](#)]
40. Panagiotopoulou, P.; Kondarides, D.I.; Verykios, X.E. Selective methanation of CO over supported Ru catalysts. *Appl. Catal. B Environ.* **2009**, *88*, 470–478. [[CrossRef](#)]
41. Petala, A.; Tsikritzis, D.; Kollia, M.; Ladas, S.; Kennou, S.; Kondarides, D.I. Synthesis and characterization of N-doped TiO₂ photocatalysts with tunable response to solar radiation. *Appl. Surf. Sci.* **2014**, *305*, 281–291. [[CrossRef](#)]
42. Panagiotopoulou, P.; Kondarides, D.I. Effects of alkali additives on the physicochemical characteristics and chemisorptive properties of Pt/TiO₂ catalysts. *J. Catal.* **2008**, *260*, 141–149. [[CrossRef](#)]
43. Hanaor, D.A.H.; Sorrell, C.C. Review of the anatase to rutile phase transformation. *J. Mater. Sci.* **2011**, *46*, 855–874. [[CrossRef](#)]
44. Alphonse, P.; Ansart, F. Catalytic coatings on steel for low-temperature propane prereforming to solid oxide fuel cell (SOFC) application. *J. Colloid Interface Sci.* **2009**, *336*, 658–666. [[CrossRef](#)]
45. Qiu, T.; Yang, J.-G.; Bai, X.-J.; Wang, Y.-L. The preparation of synthetic graphite materials with hierarchical pores from lignite by one-step impregnation and their characterization as dye absorbents. *RSC Adv.* **2019**, *9*, 12737–12746. [[CrossRef](#)]
46. Huang, W.; Li, J.; Xu, Y. Nucleation/Growth Mechanisms and Morphological Evolution of Porous MnO₂ Coating Deposited on Graphite for Supercapacitor. *Materials* **2017**, *10*, 1205. [[CrossRef](#)]

47. Kourtelesis, M.; Panagiotopoulou, P.; Ladas, S.; Verykios, X.E. Influence of the Support on the Reaction Network of Ethanol Steam Reforming at Low Temperatures Over Pt Catalysts. *Top. Catal.* **2015**, *58*, 1202–1217. [[CrossRef](#)]
48. Bradford, M.C.J.; Vannice, M.A. Catalytic reforming of methane with carbon dioxide over nickel catalysts I. Catalyst characterization and activity. *Appl. Catal. A Gen.* **1996**, *142*, 73–96. [[CrossRef](#)]
49. Guo, C.; Wu, Y.; Qin, H.; Zhang, J. CO methanation over ZrO₂/Al₂O₃ supported Ni catalysts: A comprehensive study. *Fuel Process. Technol.* **2014**, *124*, 61–69. [[CrossRef](#)]
50. Swaan, H.M.; Kroll, V.C.H.; Martin, G.A.; Mirodatos, C. Deactivation of supported nickel catalysts during the reforming of methane by carbon dioxide. *Catal. Today* **1994**, *21*, 571–578. [[CrossRef](#)]
51. Zhang, Z.L.; Tsipouriari, V.A.; Efstathiou, A.M.; Verykios, X.E. Reforming of Methane with Carbon Dioxide to Synthesis Gas over Supported Rhodium Catalysts: I. Effects of Support and Metal Crystallite Size on Reaction Activity and Deactivation Characteristics. *J. Catal.* **1996**, *158*, 51–63. [[CrossRef](#)]
52. Carlsson, M. Carbon Formation in Steam Reforming and Effect of Potassium Promotion. *Johns. Matthey Technol. Rev.* **2015**, *59*, 313–318. [[CrossRef](#)]